Journal of chemical & engineering data

Article

pubs.acs.org/jced

# Humic Acid−Fe(Hydr)oxide Composites Supported on Montmorillonite: Synthesis, Characterization, and Atrazine Adsorption

Gonzalo Bia,[†] Patricia I. Ortiz,[‡] Valeria Pfaffen,[‡] and Laura Borgnino*[,†]

[†]CICTERRA-CONICET and Universidad Nacional de Córdoba Ciudad Universitaria, 5000, Córdoba, Argentina

[‡]INFIQC - CONICET and Universidad Nacional de Córdoba Ciudad Universitaria, 5000, Córdoba, Argentina

Supporting Information

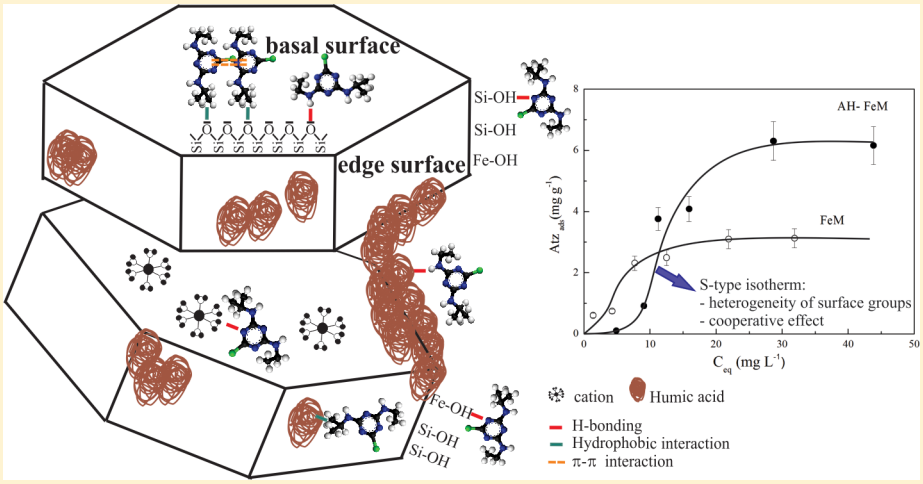


**ABSTRACT:** Much progress has been made involving the interaction of atrazine (Atz) with natural geosorbents like Fe(hydr)oxides, organic matter, and clay minerals. However, the properties of the humic acid−Fe(hydr)oxides-clay composites differ from their individual member phases, exerting an influence on the adsorption capacity and stability of the system. In this work, the evaluation of Atz adsorption onto humic acid−Fe(hydr)oxide supported on montmorillonite (HA−FeM) was performed. A combination of the X-ray diffraction pattern and batch adsorption experiments at different pH and ionic strength conditions were performed. The identification of the surface groups involved in the interaction FeM−Atz was carry out using X-ray photoelectron spectroscopy. The presence of Fe(hydr)oxides and humic acid improve the adsorption capacity of montmorillonite. Acidic pH and high ionic strength conditions further increases the adsorption. The heterogeneity of the surface sites and cooperative effect contributes to the adsorption process. However, the hydrophobic character of the herbicide is the key factor controlling adsorption. The results obtained from this work give insights about the adsorption mechanism of Atz onto humic acid Fe(hydr)oxides-clay composites and provide information about the potentiality of this type of material to be used to remove organic pollutants present in the aquatic environment.

## 1. INTRODUCTION

The herbicide atrazine (Atz) is one of the most commonly used worldwide, mostly for weed control in crops. Due to its long half-life, apparent mobility, moderate water solubility, great leaching potential, and high chemical stability in soils and aquifers, Atz has been detected in water bodies across the world.[1−3] Articles concerning human health consider Atz to be hazardous due to its high possibility of producing cancers, birth defects, and interruption of hormone functions, mainly in people who have experienced long-term exposure.[4−6] Thus, the United States, European Union, and Japan have classified Atz as an endocrine-disrupting compound. Nevertheless, it is still widely used in some developing countries.[7]

The environmental risks concerning Atz toxicity promoted a variety of studies related to its adsorption and desorption onto soils, sediments, and individual mineral particles over the last few decades. Huang et al.[8] already identified that inorganic minerals (i.e., clay minerals) organic matter and Al and Fe compounds provide surfaces sites for Atz adsorption. Since then, numerous studies have well documented the key role of humic substances as well as the importance of the mineral fraction of soils and sediments (i.e., montomorillonite and Al/

**Received:** June 5, 2017
**Accepted:** September 14, 2017





DOI: 10.1021/acs.jced.7b00504
J. Chem. Eng. Data XXXX, XXX, XXX−XXX

Fe(hydr)oxides) in the adsorption of Atz.[9−17] In the early work of Laird et al.,[9] the authors concluded that the siloxane surface groups have a high affinity for Atz. Similar conclusions were arrived by Celis et al.[10] which also informed that high surface acidity should increase the retention of s-triazine herbicides in soils. In general, the negative surface charge that clay minerals carries, the presence of basal and edge reactive surface groups, and the type of exchangeable cation present in the interlayer space make this natural material a good adsorbent to several pollutants. However, clay minerals are highly hydrophilic and consequently show very limited adsorption capacities for hydrophobic organic contaminants. Indeed, the adsorption capacity to anionic pollutants such as As(V), As(III), Cr(VI) is usually low because of the high negative charge. To overcome this, clay minerals should be modified or functionalized in order to be more selective to several organic/inorganic compounds[18−25]

The adsorption of Atz onto humic acid (HA) has been well studied. The effect of humic acid hydration on adsorption,[26,27] the interaction mechanisms[11,28] and the effect of different mono- and divalent cations have been the main topics.[14,29−31] For instance, while divalent cations usually decrease the adsorption capacity of Atz, monovalent cations may enhance it. This opposite effect responds to different behaviors: in the first case cations compete with Atz for humic acids surface sites; in the second case, cations decrease the hydrophilicity of the local region around surface sites and therefore the Atz adsorption increases.[32] The adsorption of pesticides onto Fe(hydr)oxides was also explored.[17] In the past decade, the zerovalent iron technology (ZVI or $Fe^0$) has gained attention. These synthesized materials can remove different types of groundwater pollutants.[33] However, either nano Fe hydr-(oxides) as well as humic acid particles has a strong tendency to aggregate into larger particles and therefore under these colloidal conditions the adsorption capacity is diminished because surface sites are blocked. The use of supporting material such as modified clay minerals can improve the adsorption conditions[34,35] and diminish the aggregation. Borgnino et al.[36] compared the aggregation kinetics of Fe(hydr)oxides-montmorillonite (FeM) particles under different levels of humic acid and concluded that humic acid stabilize the Fe(hydr)oxides-montmorillonite at any pH. By this way, the joint effect of the high surface area of montmorillonite along with the adsorption capacity of humic acid should enhance the adsorption of Atz, either by contributing with specific surface sites (e.g., hydrophobic sites) or as stabilizing the FeM particles.

In this article, the Atz adsorption onto a HA−Fe(hydr)oxide-montmorillonite (HA−FeM) was evaluated. In the first place, the adsorption of Atz onto Fe(hydr)oxide-montmorillonite was analyzed. X-ray photoelectron spectroscopy (XPS) and X-ray diffraction (XRD) was used to identify the surface groups involved in the interaction and the orientation of the Atz in the interlaminar space. The adsorption onto the HA−FeM system was then studied by assessing the effect of pH and ionic strength. The results obtained in this study provide insights into the understanding of the interactions involved and the adsorption capacity of Atz onto modified-montmorillonite under different conditions.

## 2. MATERIALS AND METHODS

**2.1. Reagents.** Atrazine (2-chloro-4-ethylamino-6-isopropylamine-*s*-triazine) was purchased from Sigma−Aldrich (St. Louis, MS, U.S.A.).

Humic acid was prepared from a Fluka humic acid (code: 1415-93-6), which had been previously purified according to the methodology proposed by the International Humic Substances Society.[37] Once the purification was completed, a concentrated stock solution of 2 g $L^{-1}$ was prepared by dissolving a weighed amount of HA at a pH of 10 for 2 h.

All other reagents used were of analytical (p.a.) grade.

**2.2. Synthesis of Fe(hydr)oxide-Montmorillonite and HA−Fe(hydr)oxide-Montmorillonite.** FeM was synthesized following the procedure described elsewhere[38] (see Supporting Information, S1).

For the synthesis of HA−FeM, preliminary studies of the adsorption kinetics of HA onto FeM were performed (Supporting Information, S2) to assess the conditions of the equilibration time as well as the amount of HA necessary to achieve saturation. The kinetics results show that a time of 15 h is needed to reach equilibrium. The saturation was reached for [HA] > 150 mg $L^{-1}$, and the adsorbed amount of HA was 50.0 mg HA/g FeM. The synthesis of HA−FeM was thus carried out by adding an excess of HA (200 mg $L^{-1}$); the suspension was shocked at room temperature at a pH of 9.0 and at an ionic strength of 0.1 M $NaNO_3$ for 15 h. Afterward, the suspension was centrifuged at 9000 rpm, and the solid was washed with water and dried at 60 °C. To avoid carbonate contamination, the synthesis was carried out under a $N_2$ atmosphere. The amount of HA adsorbed was 53.9 mg/g FeM, representing 5%. The detailed identification of the HA in the synthesized sample is in Supporting Information, S3.

**2.3. Characterization Methods.** *2.3.1. X-ray Diffraction.* XRD patterns were recorded with a Philips ẊPert PRO X-ray diffractometer using Cu$K_\alpha$radiation (30 kV-15 mA) and were obtained in the 2$\theta$ range from 4 to 15° (step size, 0.02; 2 seg/step). The reflection assignments were performed using the ẊPert HighScore software installed on the X- ray diffractometer.

*2.3.2. X-ray Photoelectron Spectroscopy.* XPS spectra were obtained using a Specs GmbH XR50, operated in a PHOIBOS 100 MCD Specs hemispherical electron energy analyzer with a pass energy of 40 eV and a nonmonochromatic Al K$\alpha$ source ($h\nu$ = 1486.6 eV; work voltage = 13 kV; and power = 300 W). A two-point calibration of the energy scale was performed using sputtered cleaned gold (Au $4f_{7/2}$, binding energy (BE) = 84.00 eV) and copper (Cu $2p_{3/2}$, BE = 932.67 eV) samples. The samples were analyzed in ultrahigh vacuum (UHV), and the typical base pressure in the sample chamber was in the range of 1.2−2.4 × $10^{-9}$ mbar. Broad scans were collected over a 1−1100 eV range, while high-resolution spectra for C, O, Fe, Si, Al, and Na were obtained. For energy calibration purposes, to correct charging effects all of the photoelectron peaks were referenced to the adventitious C 1s spectral component (C−C, C−H) with a binding energy of 284.8 eV. For determination of the chemical composition, data were treated with the commercial software CasaXPS (http://www.casaxps.com, Casa software) using Shirley background correction. The C, Fe, and Si spectra were fitted using the software XPS Peak 4.1 (http://www.uksaf.org/software.html#1) with peaks of the Gaussian−Lorentzian mixed function (G/L = 40) after subtraction of a Shirley baseline. The full width at half-


DOI: 10.1021/acs.jced.7b00504
J. Chem. Eng. Data XXXX, XXX, XXX−XXX

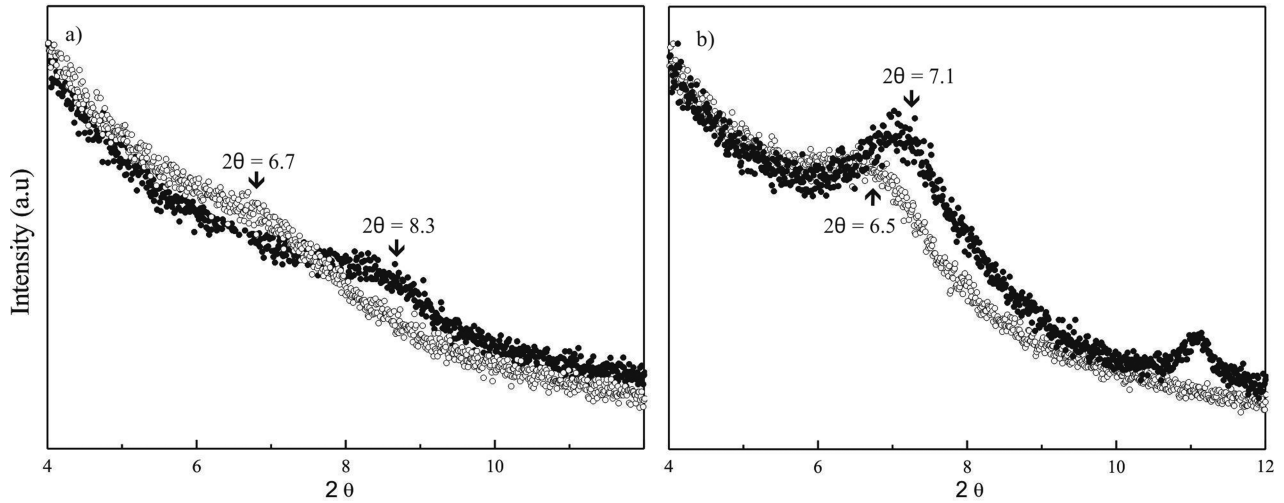


**Figure 1.** XRD patterns of (a) FeM and (b) NaM before (solid circles) and after (open circles) Atz adsorption.

maximum (fwhm) was fixed during the fitting. The fwhm's were 2.2, 3.3, 4.0, and 1.5 eV for C 1s, Fe 2p, Fe 2p satellite, and Si 2p species, respectively. To provide a reasonable agreement with the measured spectra, all spectra were fitted with the least number of components. For Fe 2p, the ratio and separation of Fe $2p_{1/2}$ and Fe $2p_{3/2}$ were restrained to the theoretical values of 1:2 and 13.6 eV, respectively.[39] Finally, peaks corresponding to the BE of C, Fe, and Si species were identified by comparing them to the reported values.

**2.4. Sorption Experiments.** The adsorption experiments were performed by suspending the sample (1 g $L^{-1}$) in $NaNO_3$ solution as a background electrolyte. After 24 h of pre-equilibration, a known volume of an Atz solution (0.4 g $L^{-1}$) prepared in the same background electrolyte was added. The Atz initial concentration range was 2−50 mg $L^{-1}$. The pH suspension was adjusted by the addition of a small amount of either $HNO_3$ or NaOH until the desired pH was obtained. After being shaken at room temperature (25.0 ± 0.5 °C) in a rotator shaker for the required time, tubes were centrifuged at 9000 rpm for 5 min, and the supernatant was separated for Atz analysis. The effects of the pH and ionic strength on Atz adsorption were also evaluated. Here, the procedure to obtain the corresponding isotherms was the same as previously described, except for the $NaNO_3$ concentrations and pH values. Three $NaNO_3$ concentrations (0.1, 0.01, and 0.001 M) at three different pH values (4.5, 7.0, and 9.0) were analyzed.

Finally, the effect of changing the cation (Na instead of Fe) in the Atz adsorption was analyzed. Adsorption experiments using NaM were performed following the same procedure as previously described.

For all adsorption experiments, measurements were performed in duplicate and the errors were around 10% .

**2.5. Atrazine and HA Quantification.** Atz quantification was determined by square wave voltammetry (SWV) with a glassy carbon electrode modified with a bismuth film. The SWV parameters and the best chemical conditions for Atz quantification were reported in Bia et al.[40] All of the electrochemical experiments were carried out with an Autolab potentiostat.

The concentration of humic acid in the solution was determined by UV spectroscopy.[41] The sample absorbance of a previously buffered solution (pH = 8.7) with 0.05 M $NaHCO_3$ was measured at 500 nm (UV−vis Shimadzu 1700).

The amounts of HA and adsorbed Atz were calculated by subtracting the measured concentration after adsorption from the initial amount added.

## 3. RESULTS AND DISCUSSION

**3.1. Atz Adsorption onto Montmorillonite: Effect of the Interlaminar Cation.** The first evidence of an interaction between Atz and the montmorillonite clay is obtained from the XRD pattern. Figure 1 presents the XRD patterns of FeM and NaM before and after Atz adsorption. As can be observed, for both samples there is an increase in the interlaminar spacing *d*. The presence of Atz is confirmed through the change in the 2$\theta$ position after Atz adsorption. For both cases, the 2$\theta$ position appears at a slightly lower angle, at approximately 6.5° and 6.7° for NaM and FeM, corresponding to basal spacings of $d_{001}$ = 13.4 and 13.2 Å, respectively. Compared with the *d*-spacings of samples without Atz (12.5 Å, 2$\theta$ = 7.1° for NaM, JCPDS 00-003-0019, and 10.7 Å, 2$\theta$ = 8.3°) for FeM), increases are observed in both cases. According to the molecular modeling proposed by Chappell et al.,[42] the orientation of the Atz molecule depends on the different hydration levels of the smectite interlayer and is related to the interacting groups involved. When the hydration is low (one layer), Atz is oriented parallel to the basal surfaces, and it interacts directly (without the intervention of water molecules) and simultaneously with hydrophobic nanosites on opposing basal surfaces. This position produces a *d*-spacing of 12.5 Å, which is close to the molecular thickness of hydrophobic molecules. For a more hydrated smectite, the Atz molecule is tilted at an acute angle relative to the basal surfaces. In this position, the two alkyl side chains interact directly with one basal surface, each by H-bonds between amino hydrogen atoms and smectite basal oxygen atoms. The rest of the Atz molecule is forced to interact with interlayer water molecules. Considering this approach and the *d*-spacing obtained here, the most probable orientation of the Atz molecule onto the montmorillonite is slightly tilted, likely interacting with siloxane groups and interlayer water molecules of the hydrated cation. This is expected to occur with the NaM sample. For the case of the FeM, the interlaminar cation added during synthesis is exchanged and precipitated as Fe(hydr)-oxide, since the pH synthesis conditions favors it.[38] In this case, it is expected that the FeOH surface group may interact with the aromatic ring of Atz through H-bonding, in a similar


DOI: 10.1021/acs.jced.7b00504
J. Chem. Eng. Data XXXX, XXX, XXX−XXX

manner as for the silanol group.[43] It is worthwhile to mention that, although Fe(hydr)oxide in FeM is present as a thin coating or very small clusters on the montmorillonite surface, interactions with the siloxane groups of montmorillonite cannot be completely avoided. These probably led to a slightly more planar configuration of the Atz molecules on the surface.

To evaluate the effect of the interlaminar cation on Atz adsorption, a comparison between Atz adsorption onto Na and FeM was performed. In Figure 2, the effect of changing the

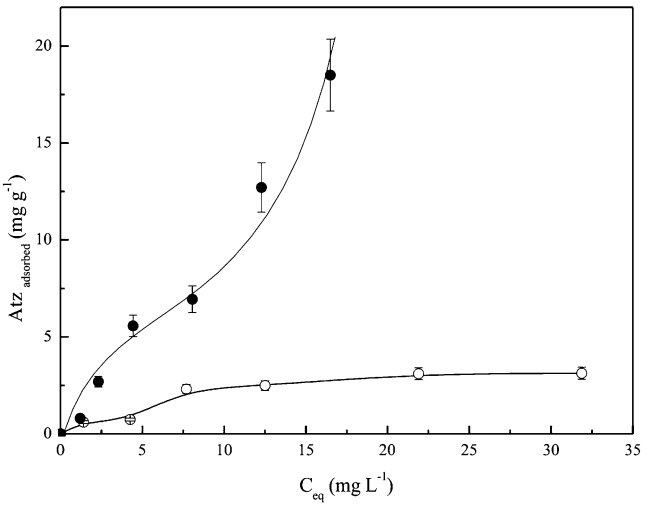


**Figure 2.** Effect of the interlaminar cation on the adsorption of Atz. Solid concentration, 1 g $L^{-1}$; pH, 7.0, and $NaNO_3$: 0.1 M. Solid circles, NaM; open circles, FeM. Lines are drawn only to serve as guides to the eyes.

interlaminar cation ($Na^+$ instead of $Fe^{3+}$) on Atz adsorption was analyzed. The isotherm curves obtained are typical for pesticide adsorption onto clays[44] and Fe(hydr)oxides.[17] The first part corresponds to a S-shaped isotherm,[45] representing an initial region of low affinity between the solid surface and the pesticide; thus, a certain amount of adsorbate is required to start the adsorption process. Afterward, a Langmuir-shaped portion is observed, reaching a plateau or pseudo plateau. The L-shape is better visualized in the FeM isotherm, perhaps due to the lower amount of Atz needed to achieve saturation. Although the shapes of the isotherms are very similar in both cases, the Atz affinity is not. Greater adsorption amounts measured for NaM (10-fold) indicate that the interlaminar cation modified the adsorption affinity. This result is different that the obtained by Herwig et al.[46] but in accordance with other studies which evaluated the effect of the hydration shell of cations on the adsorption of herbicides.[47,48] The explanation of this behavior is related to the hydrophobic character of the exchanged cation, which determines whether the molecule of Atz can get closer to the $Na^+$ or $Fe^{3+}$ cation. A greater hydration capacity suggests a lower proximity of the Atz molecule to the surface sites and thus lower adsorption. Considering that the bond length of Fe−O is 2.0 Å and the length for Na−O is 2.4 Å ($Fe^{3+}$ and $Na^+$ in their hydrated forms),[49] the hydration energy is higher for FeM, explaining the tendency of adsorption in the sense that $Na^+ > Fe^{3+}$. Although the adsorption is higher when $Na^+$ is present, the HA−metal binding depends on the cation charge and thus the affinity of $Fe^{3+}$ to HA surface groups would be higher.

### 3.2. Adsorption Mechanism of Atz onto FeM: Interactions among Surface Sites.

Figure 3 shows the characteristic C 1s, Fe 2p, and Si 2p high-resolution XPS spectra obtained for FeM before and after Atz adsorption at a pH of 4.5 and 0.1 M $NaNO_3$. The signal corresponding to N 1s could not be analyzed due to a high signal in the original sample, which is associated with the presence of N from contamination.

XPS spectra related to adsorbed aromatic nitrogen compounds often only analyze the N 1s signal, indicating the presence of the herbicide.[50] Nevertheless, the fitted curve of the XPS spectra gives additional information (i.e., the BE of the adsorbent surface groups and the atom %). In Table 1, the assignments of the BE obtained before and after the adsorption are presented; the BE shifts and changes in the atom % are marked in bold.

Figure 3a shows XPS spectra of C 1s for FeM before and after Atz adsorption (FeM−Atz), both fitted with three common contributions attributed to an amount of carbon contamination. All these peaks are detectable in most of the samples that have been exposed to the atmosphere. The first peak at 284.8 eV was taken as an internal reference and was used to correct other spectra; it corresponds to aliphatic carbon atoms (C−C and C−H groups). The second peak at approximately 286 eV is attributed to carbon in C−O single bonds. The third peak at 288.6 eV corresponds to carbon in O−C═O groups. All of the same peaks are also present in the sample with Atz; however, two new contributions are observed: a new peak at 282.5 eV attributed to C−N[51] and another one at a higher BE (near 294 eV) attributed to the $\pi-\pi^*$ shakeup transition. The peak at 282.5 eV corresponds to the C−N bond present in the aliphatic chain of the herbicide. The other peak corresponds to the signal of the delocalized electrons of the aromatic ring of the Atz molecule.[52]

The Fe 2p spectrum (Figure 3b) displays a maximum energy value at approximately 711 eV for the Fe $2p_{3/2}$ core level, together with a broad satellite peak near 719 eV. The peak at 711 eV suggests the presence of $Fe^{3+}$-O species, while peaks obtained from 712.8 to 715.4 eV correspond to a $Fe^{3+}$-multiplet. This multiplet was previously described for Fe-(hydr)oxide compounds, such as hematite, goethite, and ferrhydrite.[53,54] Particularly, the peak at 713.6 eV, which is present in FeM but not in the FeM−Atz sample, is assigned to the surface species FeOH.[55] Additionally, a slight shift in the satellite peak position was observed for the adsorbed sample. In general, a shift toward higher BE is an indication of the loss of the relative electronic density around the atom that is affected by its nearest neighbors, which in this case may be due to the presence of adsorbed Atz.

The peak sequence between 102.2 and 103.8 eV in the Si 2p spectrum (Figure 3c) corresponds to Si bonded to two, three, and four oxygen atoms.[56] Most of these peaks appear in both samples and correspond to Si in a silicate environment and could be interpreted as the siloxane surface group of montmorillonite. The peak at approximately 104−105 eV indicates the presence of SiOH (silanol) surface groups.[57] It can be seen from Table 1 that the position of the Si 2p contribution shifted to higher values by 0.4 and 0.5 eV after Atz adsorption. This shift in the Si 2p position is evidence of a change in the physical−chemical environment around the Si atoms, likely related to the interaction between siloxane and/or silanol groups with Atz.


DOI: 10.1021/acs.jced.7b00504
J. Chem. Eng. Data XXXX, XXX, XXX−XXX

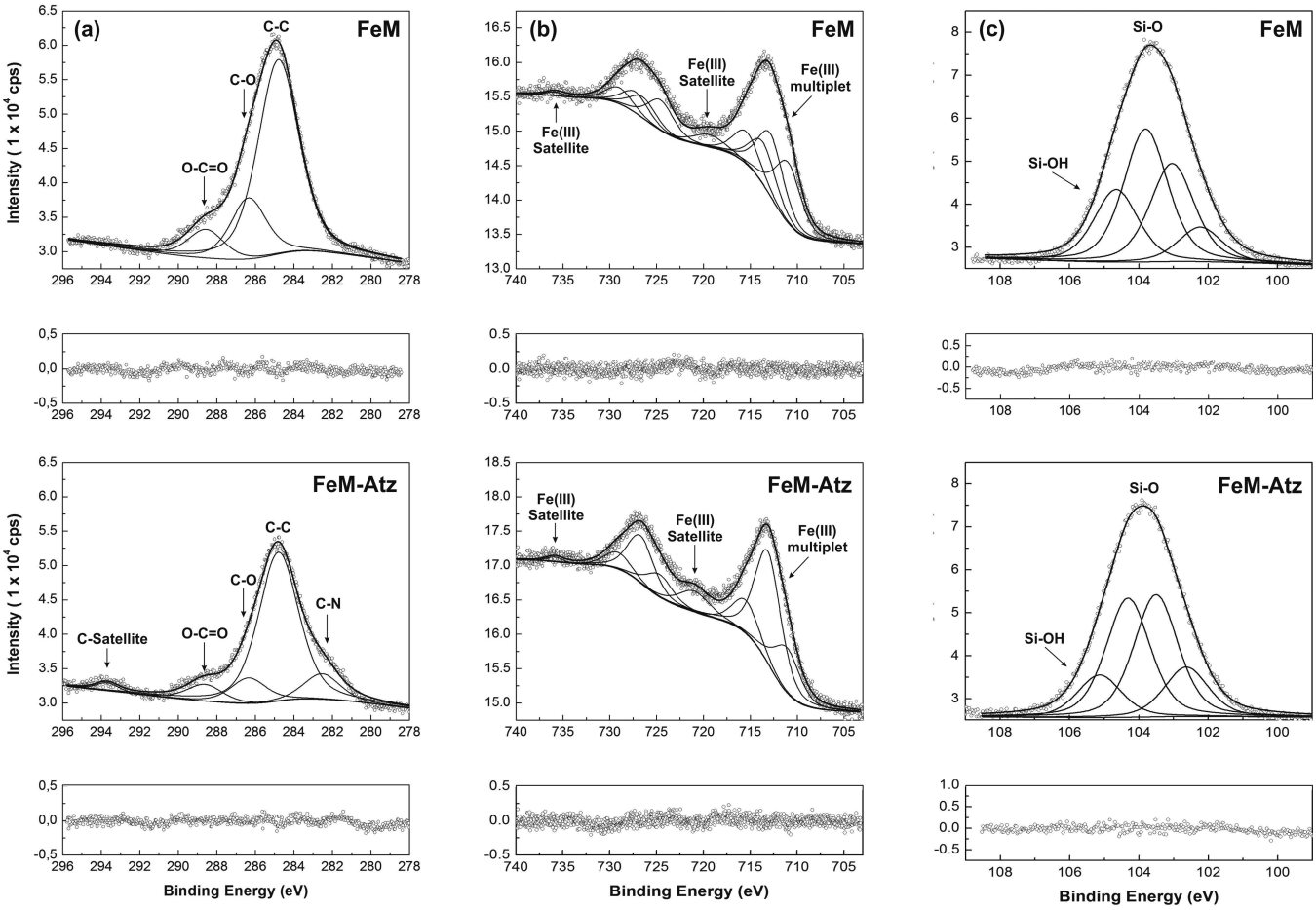


**Figure 3.** X-ray photoelectron (a) C 1s, (b) Fe 2p, and (c) Si 2p spectra obtained for FeM samples before and after the adsorption of Atz. The original spectra are indicated with empty circles. The best fit curves and individual peaks are shown by a solid thick line. The residuals plots presented below the spectra provided the error associated with the fitting process.

**Table 1. BE Assignments and Atom % for C 1s, Fe $2p_{3/2}$, and Si 2p Elements before and after Atz Adsorption**

| | | FeM | | FeM-Atz | | |
|---|---|---|---|---|---|---|
| species | | BE (eV) | Atom % | BE (eV) | atom % | assignment |
| | C−N | | | **282.5** | **1.2** | C−N |
| C 1s | C−C | 284.8 | 11.1 | 284.8 | 7.7 | aliphatic carbon |
| | C−O | 286.3 | 3.0 | 286.4 | 1.2 | adventitious carbon contamination |
| | O−C═O | 288.6 | 1.4 | 288.6 | 0.8 | |
| | C-Satellite | | | **293.7** | **0.2** | $\pi-\pi^*$ shakeup transition |
| Fe $2p_{3/2}$ | $Fe^{3+}$-O | 711.0 | 0.4 | 711.1 | 0.3 | $Fe^{3+}$ in Fe oxides |
| | $Fe^{3+}$-multiplet | 712.8 | 0.4 | 713.1 | 0.7 | Fe−OH specie |
| | $Fe^{3+}$-multiplet | **713.6** | **0.3** | | | |
| | $Fe^{3+}$-multiplet | 715.4 | 0.2 | 715.5 | 0.2 | |
| | Fe $^{3+}$ satellite | **719.4** | 0.1 | **721.0** | 0.1 | |
| Si 2p | $Si(-O_2)$ | **102.2** | 2.3 | **102.6** | 3.3 | Si in silicate environment |
| | $Si(-O_3)$ | **103.0** | 6.4 | **103.5** | 8.1 | |
| | $Si(-O_4)$ | **103.8** | 8.7 | **104.3** | 7.9 | |
| | Si−OH | **104.7** | **4.7** | **105.1** | **2.8** | SiOH specie |
| $C_{Total}$ | | | 15.5 | | 11.1 | |
| $Si_{Total}$ | | | 22.1 | | 22.1 | |
| $Fe_{Total}$ | | | 1.4 | | 1.3 | |
| $O_{Total}$ | | 532.5 | 52.8 | 532.3 | 55.6 | |
| $Al_{Total}$ | | 74.7 | 6.8 | 74.8 | 6.8 | |
| $Na_{Total}$ | | 1073.3 | 1.4 | 1073.0 | 3.1 | |

According to the obtained XPS results, two important facts can be remarked. First, the presence of Atz is evidenced through the C−N signal, $\pi-\pi^*$ shakeup transition, and slight shifts in the Si 2p and Fe $2p_{3/2}$ (satellite) spectra, which are all



DOI: 10.1021/acs.jced.7b00504
J. Chem. Eng. Data XXXX, XXX, XXX−XXX

attributed to the presence of Atz near the surface region of FeM. In the second term, in accordance with the changes in the atom % of Si 2p and Fe 2p3/2 atoms the silanol and FeOH groups are involved in the interaction with Atz, probably by H-bonding with the N-aromatic ring. In both cases, the interaction would be deduced from changes in the atom %. For the silanol (4.7 to 2.8%) and FeOH (0.3 to 0%) groups, there is a decrease in the atom % as a consequence of the presence of Atz in the region near the surface that masks those surface groups (Table 1). The H-bonding interaction between the siloxane and NH group has already been implied through XRD results. However, XPS cannot reveal this interaction; in fact, there is an increase in the atom % of the Si−O−Si group after Atz adsorption. This result was interpreted as a more open interlayer space allowing more exposition of the siloxane groups.

Although XPS does not allow confirmation of the n-$\pi$ EDA interactions, these are less probable to occur because of the tilt orientation of the Atz molecule. The $\pi-\pi$ interactions between the aromatic groups of Atz molecules are more likely to be present. Indeed, this type of interaction would be present, as the tilt orientation of the Atz molecule favors lateral interactions between the aromatic rings, increasing the adsorption by cooperative effects (see the next section).

**3.3. Effect of Humic Acid on Atz Adsorption: pH and Ionic Strength Condition.** Similar for Atz adsorption onto Na and FeM, the adsorption onto the HA−FeM system resembles an S-type adsorption isotherm (Figure 4). The

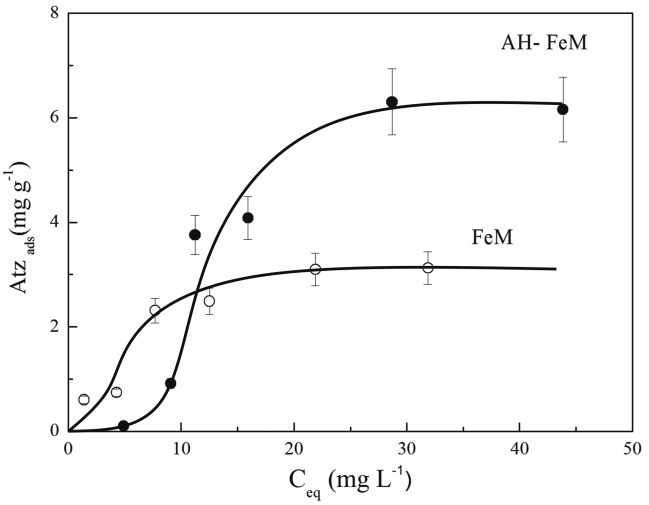


**Figure 4.** Comparison of the adsorption behavior of Atz on FeM and HA−FeM. Solid concentration, 1 g $L^{-1}$; pH, 7.0; and $NaNO_3$, 0.1 M. Lines are drawn only to serve as guides to the eyes.

heterogeneity of surface sites and cooperative effect are responsible for the curve shape. Cooperative adsorption operates if adsorbate−adsorbate interactions are stronger than adsorbate−adsorbent interactions. At low concentrations, the adsorbate has a low affinity for the adsorbent, but as soon as the adsorbate is covered, other molecules are more easily adsorbed.[58,59] This phenomenon is frequently observed for organic molecules, surfactants,[60,62] and Fe(hydr)oxides, such as goethite.[17] Figure 4 presents Atz adsorption isotherms onto FeM and HA−FeM samples. Both are S-type isotherm. The HA molecule provided more, other, or better surface adsorption sites and therefore the adsorption capacity of the FeM system increases in 3-fold. Regarding the possible order of the occupation of surface sites, it is expected that at low Atz concentrations, the interaction occurs preferentially onto FeM sites, as they predominate over humic acid sites. When the Atz concentration increases, the herbicide is also adsorbed onto HA surface sites.

Figure 5 shows Atz adsorption onto HA−FeM at three different pH values. The analyzed pH range represents the

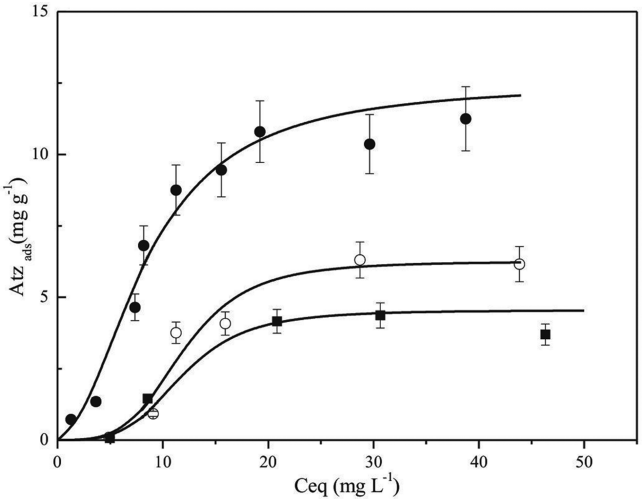


**Figure 5.** Effect of the pH on Atz adsorption on HA−FeM. Solid concentration, 1 g $L^{-1}$; $NaNO_3$; 0.1 M. Solid circles, pH = 4.5; open circles, pH = 7.0; squares, pH = 9.0.

entire pH range to evaluate the adsorption under different potential environmental conditions. As can be observed in Figure 5, there is an increase in adsorption as the pH decreases. In this case, the pH affects not only the HA−FeM surface charge but also the HA conformation and Atz molecule protonation, which are all factors influencing the adsorption capacity. First, at low pH values HA molecules aggregate in a more compact conformation, producing an enhancement of the hydrophobic character, which implies greater Atz adsorption.[14] Additionally, N in the Atz aromatic ring can form H-bonding with HA carboxylic and phenolic groups. Therefore, the hydrophobic effect and H-bonding interactions clearly favor the adsorption process. Additionally, a low pH contributes to generate some reduction in the electrostatic repulsion between Atz and HA−FeM. Although the Atz molecule is neutral at the pH values studied, chloride and the negative electronic density of the Atz aromatic ring may generate some repulsion between Atz and HA−FeM. Surface site protonation (i.e., FeOH sites in FeM as well as carboxylic and phenolic groups in the HA molecule) reduce the electrostatic repulsion. In fact, as can be seen in Figure 5, for pH 4.5 there is a rapid increase in Atz adsorption, suggesting that pH really enhances the adsorption capacity. However, at pH 7.0 and 9.0, and at low initial concentrations, the amounts of Atz adsorbed are lower and similar among these pH values. At these pH values, the net negative surface charges of FeM and HA molecules remain negative, and thus reduction in the electrostatic repulsion cannot be avoided. Nevertheless, the adsorption capacity at pH 7.0 (~6 mg $g^{-1}$) is higher than other similar systems based on modification of montmorillonite with HA, organoclays, or geosorbent materials.[61−66]

Adsorption models, such as the Langmuir and Freundlich isotherms, have been widely used to evaluate adsorption


DOI: 10.1021/acs.jced.7b00504
J. Chem. Eng. Data XXXX, XXX, XXX−XXX

phenomena. Generally, experimental data are fit to adsorption isotherm models, and the obtained parameters are then used to describe the adsorption process. In the literature, different isotherm models were used to explain the adsorption behavior of pesticides. In general, pesticide binding to HA, Fe(hydr)-oxides, and clays can be described with the Freundlich equation.[14,67] The Langmuir model has been used less frequently.[68] Ishiguro et al.[69] evaluated the adsorption of a cation surfactant onto HA using a combination of an electrostatic and specific binding adsorption model. The specific model is the Langmuir−Freundlich-Hill (LFH) and is described as follows

$$X_s = X^m \frac{(K_s C_s)^n}{1 + (K_s C_s)^n}$$

Similar to the Freundlich model, the Langmuir−Freundlich-Hill (LFH) model includes a $n$ parameter in the equation. For the Freundlich model, the $n$ parameter is a measure of the heterogeneity of the system. A more homogeneous system will have $n$ values approaching unity, while in more heterogeneous systems, $n$ values will approach zero. The meaning of $n$ is somewhat different in the LFH model. According to Ishiguro et al.,[69] if $n < 1$, the heterogeneity effects are larger than the hydrophobic effects, while for $n > 1$, the hydrophobic attraction is stronger than the heterogeneity effects. Pseudoideality ($n = 1$) occurs when effects, heterogeneity and hydrophobicity, compensate for each other. Atz adsorption behavior onto HA−FeM would be similar to that of surfactants onto HA since both the heterogeneity of the binding sites (previously discussed) and a positive cooperative effect due to hydrophobic attraction play important roles. Therefore, this model was used here but just for the purpose of fitting experimental data and finding the $n$ value assigned to the adsorption process. Any other interpretation is beyond the scope of this paper. Figure 5 shows that the model presents a good fit with the experimental data. The obtained $n$ values in all of the cases were >1 (Table S2), suggesting that the hydrophobic effect is more important than the heterogeneity effect. These results indicate that more than the surface sites available for adsorption, the hydrophobic characters of the adsorbate and adsorbent are controlling the adsorption process. In this regard, increasing the hydrophobicity increases adsorption on the Fe-coated clay. Finally, the ionic strength clearly contributes to the adsorption process (Figure 6). High ionic strength influences both the HA molecule conformation and electrostatic interactions. The HA molecules show a more compressed conformation at high ionic strength, leading to smaller-sized aggregates. Moreover, high ionic strength reduces the thickness of the electrical double layer, which favors $\pi-\pi$ stacking between the aromatic rings; thus, Atz adsorption increases by a cooperative effect.

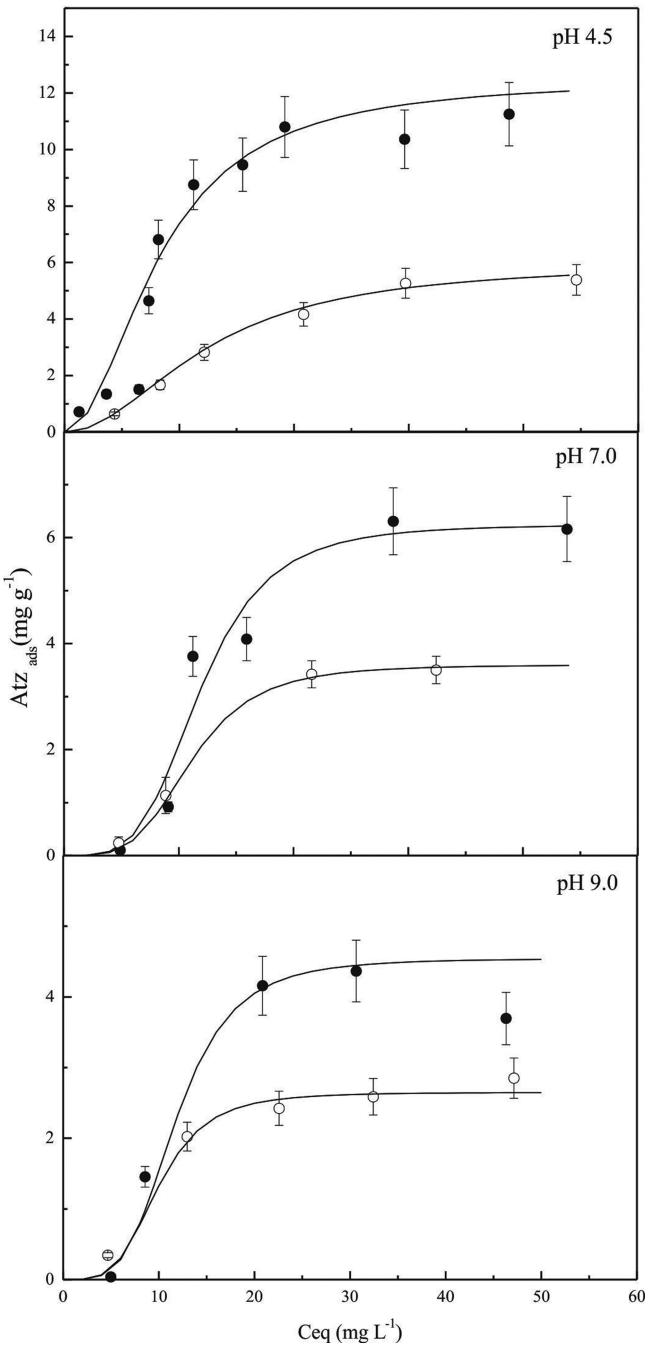


**Figure 6.** Effect of the ionic strength on the adsorption of Atz onto HA−FeM. Solid circles, 0.1 M $NaNO_3$; open circles, 0.01 M $NaNO_3$.

## CONCLUSIONS

This paper attempts to advance the knowledge of the adsorption mechanism of Atz onto geosorbents and to determine the effects of the pH, humic acid, and ionic strength in this process. The obtained results allow it to be concluded that Atz is adsorbed onto Na and FeM. The interlaminar cation influences the adsorption capacity of the montmorillonite in the sense that $Na^+ > Fe^{3+}$.

The XPS spectroscopy tool confirmed the presence of Atz in the near surface region of FeM. The silanol and FeOH groups are involved in the interaction; thus, H-bonding with the N-aromatic group would be the expected interaction. The tilted orientation of the Atz molecules in the interlayer space, deduced from XRD patterns, facilitate the H-bonding interactions. Additionally, the $\pi-\pi$ stacking interactions contribute to the adsorption process through a cooperative effect.

Smectites adsorb low amount of Atz; however, in the presence of Fe(hydr)oxides the adsorption is improved. The effect of humic acid is to further increase the adsorption capacity. The heterogeneity of the surface sites and the cooperative effect explained the S-type curve observed in the HA−FeM adsorption isotherms. However, the hydrophobic character of the herbicide seems to be the key factor for the


DOI: 10.1021/acs.jced.7b00504
J. Chem. Eng. Data XXXX, XXX, XXX−XXX

adsorption process. Acidic pH values and high ionic strengths also increase Atz adsorption.

## ■ ASSOCIATED CONTENT

### Supporting Information

The Supporting Information is available free of charge on the ACS Publications website at DOI: 10.1021/acs.jced.7b00504.

Synthesis of FeM and adsorption kinetic of HA onto FeM; identification of HA in the HA−FeM sample; parameters obtained after fit adsorption data using LFH model (PDF)

## ■ AUTHOR INFORMATION


### Corresponding Author

*E-mail: lauraborgnino@gmail.com.

### ORCID

Laura Borgnino: 0000-0002-5592-3422



### Funding

The authors wish to acknowledge the assistance of CONICET and UNC, whose support facilities and funds were used in this investigation. G.B. acknowledges a doctoral fellowship from CONICET. L.B., P.O., and V.P. are members of CICyT in CONICET, the National Science Foundation of Argentina.


### Notes

The authors declare no competing financial interest.

## ■ REFERENCES


(1) Graymore, M.; Stagnitti, F.; Allinson, G. Impacts of atrazine in aquatic ecosystems. *Environ. Int.* **2001**, *26*, 483−495.

(2) Steele, G. V.; Johnson, H. M.; Sandstrom, M. W.; Capel, P. D.; Barbash, J. E. Occurrence and fate of pesticides in four contrasting agricultural settings in the United States. *J. Environ. Qual.* **2008**, *37*, 1116−1132.

(3) Kucka, M.; Pogrmic-Majkic, K.; Fa, S.; Stojilkovic, S. S.; Kovacevic, R. Atrazine acts as an endocrine disrupter by inhibiting cAMP-specific phosphodiesterase-4. *Toxicol. Appl. Pharmacol.* **2012**, *265*, 19−26.

(4) Zaya, R. M.; Amini, Z.; Whitaker, A. S.; Kohler, S. L.; Ide, C. F. Atrazine exposure affects growth, body condition and liver health in Xenopus laevis tadpoles. *Aquat. Toxicol.* **2011**, *104*, 243−253.

(5) Kirkley, A. G.; Sargis, R. M. Environmental endocrine disruption of energy metabolism and cardiovascular risk. *Curr. Diabetes Rep.* **2014**, *14*, 494−456.

(6) Papoulias, D. M.; Tillitt, D. E.; Talykina, M. G.; Whyte, J. J. Atrazine reduces reproduction in Japanese medaka (Oryzias latipes). *Aquat. Toxicol.* **2014**, *154*, 230−239.

(7) U.S. EPA, 2013. Atrazine Updates In: Pesticides Registration. http://www.epa.gov/pesticides/reregistration/atrazine/atrazine-update.htm (last access date on August 7th, 2017).

(8) Huang, P. M.; Grover, M.; McKercher, R. B. Components and particle size fraction involved in atrazine adsorption by soils. *Soil Sci.* **1984**, *138*, 20−24.

(9) Laird, D. A.; Koskinen, W. Triazine Soil Interactions. In *The Triazine Herbicides*; LeBaron, H. M., McFarland, J. E., Burnside, O. C., Ed.; Elsevier, 2008; pp 275−299.

(10) Celis, R.; Cornejo, J.; Hermosin, M. C.; Koskinen, W. C. Sorption-desorption of Atrazine and Simazide by model soil colloidal components. *Soil Sci. Soc. Am. J.* **1997**, *61*, 436−443.

(11) Martin-Neto, L.; et al. Mechanism of Atrazine Sorption by Humic Acid: A Spectroscopic Study. *Environ. Sci. Technol.* **1994**, *28*, 1867−1873.

(12) Keiluweit, M.; Kleber, M. Molecular-Level Interactions in Soils and Sediments: The Role of Aromatic π-Systems. *Environ. Sci. Technol.* **2009**, *43*, 3421−3429.

(13) Lu, J.; Li, Y.; Yan, X.; Shi, B.; Wang, D.; Tang, H. Sorption of atrazine onto humic acids (HAs) coated nanoparticles. *Colloids Surf., A* **2009**, *347*, 90−96.

(14) Kovaios, I. D.; Paraskeva, C. A.; Koutsoukos, P. G. Adsorption of atrazine from aqueous electrolyte solutions on humic acid and silica. *J. Colloid Interface Sci.* **2011**, *356*, 277−285.

(15) He, Y. Y.; Wang, X. C. Adsorption of a typical polycyclic aromatic hydrocarbon by humic substances in water and the effect of coexisting metal ions. *Colloids Surf., A* **2011**, *379*, 93−101.

(16) Mudhoo, A.; Garg, V. K. Sorption, Transport and Transformation of Atrazine in Soils. Minerals and Composts: A Review. *Pedosphere* **2011**, *21*, 11−25.

(17) Arce, F.; Iglesias, A. C.; López, R.; Gondar, D.; Antelo, J.; Fiol, S. Interactions Between Ionic Pesticides and Model Systems for Soil Fractions. In *Pesticides in the Modern World - Risks and Benefits*; Stoytcheva, M., Ed.; In Tech, 2011.

(18) Alther, G. R. Organically modified clay removes oil from water. *Waste Manage.* **1995**, *15*, 623−628.

(19) Jiang, J. Q.; Cooper, C.; Ouki, S. Comparision of modified montmorillonite adsorbents. Part I. Preparation, characterization and phenol adsorption. *Chemosphere* **2002**, *47*, 711−716.

(20) Smith, J.; Bartelt-Hunt, S.; Burns, S. Sorption and permeability of gasoline hydrocarbons in organobentonites porous media. *J. Hazard. Mater.* **2003**, *96*, 91−97.

(21) Lee, S. M.; Tiwari, D. Organo and inorgano-organo-modified clays in the remediation of aqueous solutions: An overview. *Appl. Clay Sci.* **2012**, *59−60*, 84−102.

(22) Liu, H.; Chen, W.; Liu, C.; Liu, Y.; Dong, C. Magnetic mesoporous clay adsorbent: Preparation, characterization and adsorption capacity for atrazine. *Microporous Mesoporous Mater.* **2014**, *194*, 72−78.

(23) Unuabonah, E. I.; Taubert, A. Clay−polymer nanocomposites (CPNs): Adsorbents of the future for water treatment. *Appl. Clay Sci.* **2014**, *99*, 83−92.

(24) Grundgeiger, E.; Hong Lim, Y.; Frost, R. L.; Ayoko, G. A.; Xi, Y. Application of organo-beidellites for the adsorption of atrazine. *Appl. Clay Sci.* **2015**, *105−106*, 252−258.

(25) Chen, L.; Zhou, C. H.; Fiore, S.; Shen Tong, D.; Zhang, H.; Sheng, Li C.; Sheng, Ji F.; Yu, W. H. Functional magnetic nanoparticle/clay mineral nanocomposites: preparation, magnetism and versatile applications. *Appl. Clay Sci.* **2016**, *127−128*, 143−163.

(26) Graber, E. R.; Borisover, M. D. Hydration-Facilitated Sorption of Specifically Interacting Organic Compounds by Model Soil Organic Matter. *Environ. Sci. Technol.* **1998**, *32*, 258−263.

(27) Borisover, M. D.; Graber, E. R. Simplified Link Solvation Model (LSM) for Sorption in Natural Organic Matter. *Langmuir* **2002**, *18*, 4775−4782.

(28) Davies, J. E. D.; Jabeen, N. The Adsorption of Herbicides and Pesticides on Clay Minerals and Soils. Part 2. Atrazine J. Inclusion Phenom. *J. Inclusion Phenom. Mol. Recognit. Chem.* **2003**, *46*, 57−64.

(29) Chen, J.; Zhu, D.; Sun, C. Effect of Heavy Metals on the Sorption of Hydrophobic Organic Compounds to Wood Charcoal. *Environ. Sci. Technol.* **2007**, *41*, 2536−2541.

(30) Chen, G.-C.; Shan, Q.-X.; Wang, Y.-S.; Pei, Z.; Shen, X.-E.; Wen, B.; Owens, G. Effects of Copper, Lead, and Cadmium on the Sorption and Desorption of Atrazine onto and from Carbon Nanotubes. *Environ. Sci. Technol.* **2008**, *42*, 8297−8302.

(31) Wang, Y.; Pei, Z.; Shan, X.; Chen, G.; Zhang, J.; Xie, Y.; Zheng, L. Effects of metal cations on sorption-desorption of p-nitrophenol onto wheat ash. *J. Environ. Sci.* **2011**, *23*, 112−118.

(32) Liu, Z.; Guo, H.; He, H.; Sun, C. Sorption and cosorption of the nonionic herbicide mefenacet and heavy metals on soil and its components. *J. Environ. Sci.* **2012**, *24*, 427−434.

(33) Ezzatahmadi, N.; Ayoko, G. A.; Millar, G. J.; Speight, R.; Yan, C.; Li, J.; Li, S.; Zhu, J.; Xi, Y. Clay-supported nanoscale zero-valent iron composite materials for the remediation of contaminated aqueous solutions: A review. *Chem. Eng. J.* **2017**, *312*, 336−350.

(34) Bhowmick, S.; Chakraborty, S.; Mondal, P.; Van Renterghem, W.; Van den Berghe, S.; Roman-Ross, G.; Chatterjee, D.; Iglesias, M.




DOI: 10.1021/acs.jced.7b00504
J. Chem. Eng. Data XXXX, XXX, XXX−XXX

Montmorillonite-supported nanoscale zero-valent iron for removal of arsenic from aqueous solution: kinetics and mechanism. *Chem. Eng. J.* **2014**, *243*, 14−23.
(35) Li, Y.; Zhang, Y.; Li, J.; Sheng, G.; Zheng, X. Enhanced reduction of chlorophenols by nanoscale zerovalent iron supported on organobentonite. *Chemosphere* **2013**, *92*, 368−374.
(36) Borgnino, L. Experimental determination of the colloidal stability of Fe(III)-montmorillonite: Effects of organic matter, ionic strength and pH conditions. *Colloids Surf., A* **2013**, *423*, 178−187.
(37) Sparks, D. L. *Methods of Soil Analysis*; Soil Science Society of America: American Society of Agronomy: Madison, WI, 1996
(38) Borgnino, L.; Avena, M.; De Pauli, C. P. Synthesis and characterization of Fe(III)-montmorillonites for phosphate adsorption. *Colloids Surf., A* **2009**, *341*, 46−52.
(39) Wagner, C. D.; Riggs, W. M.; Davis, L. E.; Moulder, J. F.; Muilenberg, G. E. *Handbook of X-Ray Photoelectron Spectroscopy*; Perkin-Elmer Corporation, Physical Electronics Division: Eden Prairie, MN, 1997
(40) Bia, G.; Borgnino, L.; Ortiz, P. I.; Pfaffen, V. Multivariate optimization of square wave voltammetry using bismuthfilm electrode to determine atrazine. *Sens. Actuators, B* **2014**, *203*, 396−405.
(41) Vermeer, A. W. P.; Van Riemsdijk, W. H.; Koopal, L. K. Adsorption of humic acid to mineral particles. 1: specific and electrostatic interactions. *Langmuir* **1998**, *14*, 2810−2819.
(42) Chappell, M.; Laird, D.; Thompson, M.; Li, H.; Teppen, B. J.; Aggarwal, V.; Johnston, C.; Boyd, S. Influence of smectite hydration and swelling on atrazine sorption behavior. *Environ. Sci. Technol.* **2005**, *39*, 3150−3156.
(43) Ringwald, C. S.; Pemberton, J. Adsorption interactions of aromatics and heteroaromatics with hydrated and dehydrated silica surfaces by raman and FTIR spectroscopies. *Environ. Sci. Technol.* **2000**, *34*, 259−265.
(44) Sawhney, B. L.; Singh, S. S. Sorption of atrazine by A1- and Ca-saturated smectite. *Clays Clay Miner.* **1997**, *45*, 333−338.
(45) Inacio, J.; Taviot-Gueho, C.; Forano, C.; Besse, J. P. Adsorption of MCPA pesticide by Mg Al-layered double hydroxides. *Appl. Clay Sci.* **2001**, *18*, 255−264.
(46) Herwig, U.; Klumpp, E.; Narres, H.-D.; Schwuger, M. J. Physicochemical interactions between atrazine and clay minerals. *Appl. Clay Sci.* **2001**, *18*, 211−222.
(47) Sheng, G.; Johnston, C. T.; Teppen, B. J.; Boyd, S. A. Adsoprtion of dinitrophenol herbicides from water to montmorillonites. *Clays Clay Miner.* **2002**, *50*, 25−34.
(48) Chen, G. C.; Shan, X.-Q.; Wang, Y.-S.; Pei, Z.-G.; Shen, X.-E.; Wen, B.; Owens, G. Effects of Copper, Lead, and Cadmium on the Sorption and Desorption of Atrazine onto and from Carbon Nanotubes. *Environ. Sci. Technol.* **2008**, *42*, 8297−8302.
(49) Richens, D. *The Chemistry of Aqua Ions*; John Wiley and Sons: Chichester, U.K., 1997
(50) Lombardi, B. M.; Torres Sanchez, R. M.; Eloy, P.; Genet, M. Interaction of thiabendazole and benzimidazole with montmorillonite. *Appl. Clay Sci.* **2006**, *33*, 59−65.
(51) Park, Y.; Ayoko, G. A.; Frost, R. L. Characterization of organoclays and adsorption of p-nitrophenol: Environmental application. *J. Colloid Interface Sci.* **2011**, *360*, 440−456.
(52) Mikhailik, O. M.; Pankratov, Y. V.; Bakai, E. A.; Senkevich, A. I.; Shpak, A. P. Surface structure of finely dispersed iron stabilized by spontaneous adsorption as derived from XPS and ESR evidence. *J. Electron Spectrosc. Relat. Phenom.* **1995**, *76*, 695−702.
(53) Grosvenor, A. P.; Kobe, B. A.; Biesinger, M. C.; McIntyre, N. S. Investigation of multiplet splitting of Fe 2p XPS spectra and bonding in iron compounds. *Surf. Interface Anal.* **2004**, *36*, 1564−1574.
(54) Biesinger, M. C.; Payne, B. P.; Grosvenor, A. P.; Lau, L. W. M.; Gerson, A. R.; Smart, R.St.C. Resolving surface chemical states in XPS analysis of first row transition metals, oxides and hydroxides: Cr, Mn, Fe, Co and Ni. *Appl. Surf. Sci.* **2011**, *257*, 2717−2730.
(55) Harun, M. K.; Lyon, S. B.; Marsh, J. A. A surface analytical study of functionalised mild steel for adhesion promotion of organic coatings. *Prog. Org. Coat.* **2003**, *46*, 21−27.
(56) Brookes, P. N.; Fraser, S.; Short, R. D.; Hanley, L.; Fuoco, E.; Roberts, A.; Hutton, S. The effect of ion energy on the chemistry of air-aged polymer films grown from the hyperthermal polyatomic ion $Si_2OMe_5^+$. *J. Electron Spectrosc. Relat. Phenom.* **2001**, *121*, 281−297.
(57) Paparazzo, E.; Fanfoni, M.; Severini, E. Studies on the structure of the $SiO_x/SiO_2$ interface. *Appl. Surf. Sci.* **1992**, *56*−*58*, 866−872.
(58) Karimi-Lotfabad, S.; Pickard, M. A.; Gray, M. R. Reactions of polynuclear aromatic hydrocarbons on soil. *Environ. Sci. Technol.* **1996**, *30*, 1145−1151.
(59) Pignatello, J. J. The measurement and interpretation of sorption and desorption rates for organic compounds in soil media. *Adv. Agron.* **1999**, *69*, 1−73.
(60) Smith, J. A.; Galan, A. Sorption of non-ionic organic contaminants to single and dual organic cation bentonite from water. *Environ. Sci. Technol.* **1995**, *29*, 685−692.
(61) Groisman, L.; Rav-Acha, C.; Gerstl, Z.; Mingelgrin, U. Sorption of organic compounds of varying hydrophobicities from water and industrial waste water by long- and short chain orgnaoclays. *Appl. Clay Sci.* **2004**, *24*, 159−166.
(62) Besse-Hoggan, P.; Alekseeva, T.; Sancelme, M.; Delort, A.-M.; Forano, C. Atrazine biodegradation modulated by clays and clay/humic acid complexes. *Environ. Pollut.* **2009**, *157*, 2837−2844.
(63) Sánchez-Jiménez, N.; Sevilla, M. T.; Cuevas, J.; Rodríguez, M.; Procopio, J. R. Interaction of organic contaminants with natural clay type geosorbents: Potential use as geologic barrier in urban landfill. *J. Environ. Manage.* **2012**, *95*, S182−S187.
(64) Abate, G.; Masini, J. C. Adsorption of atrazine, hydroxyatrazine, deethylatrazine, and deisopropylatrazine onto Fe(III) polyhydroxy cations intercalated vermiculite and montmorillonite. *J. Agric. Food Chem.* **2005**, *53*, 1612−1619.
(65) Park, Y.; Sun, Z.; Ayoko, G. A.; Frost, R. L. Removal of herbicides from aqueous solutions by modified forms of montmorillonite. *J. Colloid Interface Sci.* **2014**, *415*, 127−132.
(66) Deng, H.; Feng, D.; He, J.-X.; Li, F.-X.; Yu, H.-M.; Ge, C.-M. Influence of biochar amendments to soil on the mobility of atrazine using sorption-desorption and soil thin-layer chromatography. *Ecol. Eng.* **2017**, *99*, 381−390.
(67) Zhang, L.; Luo, L.; Zhang, S. Adsorption of phenanthrene and 1,3-dinitrobenzene on cation-modified clay Minerals. *Colloids Surf., A* **2011**, *377*, 278−283.
(68) Marco-Brown, J. L.; Areco, M. M.; Torres Sánchez, R. M.; dos Santos Afonso, M. Adsorption of picloram herbicide on montmorillonite: Kinetic and equilibrium studies. *Colloids Surf., A* **2014**, *449*, 121−128.
(69) Ishiguro, M.; Koopal, L. K. Predictive model of cationic surfactant binding to humic substances. *Colloids Surf., A* **2011**, *379*, 70−78.


DOI: 10.1021/acs.jced.7b00504
*J. Chem. Eng. Data* XXXX, XXX, XXX−XXX